Catalysis Today 143 (2009) 51–56

Contents lists available at ScienceDirect

Catalysis Today

journal homepage: www.elsevier.com/locate/cattod

Influence of Zn concentration in the activity of $Cd_{1-x}Zn_xS$ solid solutions for water splitting under visible light

F. del Valle [a], A. Ishikawa [b], K. Domen [b], J.A. Villoria de la Mano [a], M.C. Sánchez-Sánchez [a], I.D. González [a], S. Herreras [a], N. Mota [a], M.E. Rivas [a], M.C. Álvarez Galván [a], J.L.G. Fierro [a], R.M. Navarro [a,*]

[a] Instituto de Catálisis y Petroleoquímica (CSIC), C/Marie Curie 2, 28049, Madrid, Spain
[b] Department of Chemical System Engineering, School of Engineering, The University of Tokyo 7-3-1 Hongo, Bunkyo-Ku, Tokyo 113-8656, Japan

ARTICLE INFO

Article history:
Available online 17 November 2008

Keywords:
Cadmium sulfide
Zinc sulfide
Solid solutions
Photocatalyst
Hydrogen
Water splitting

ABSTRACT

Solid solutions $Cd_{1-x}Zn_xS$ with different Zn concentration ($0.2 < x < 0.35$) are investigated in the production of hydrogen from aqueous solutions containing SO_3^{2-}/S^{2-} as sacrificial reagents under visible light. Textural, structural and surface catalyst properties are determined by N_2 adsorption isotherms, UV–vis spectroscopy, SEM and XRD and related to the activity results in hydrogen production from water splitting under visible light irradiation. It is found that the crystallinity and energy band structure of the $Cd_{1-x}Zn_xS$ solid solutions depend on their Zn atomic concentration. The hydrogen production rate is found to increase gradually when the Zn concentration on photocatalysts increases from 0.2 to 0.3. Subsequent increase in the Zn fraction up to 0.35 leads to lower hydrogen production. Variation in photoactivity is analyzed in terms of changes in crystallinity, level of conduction band and light absorption ability of $Cd_{1-x}Zn_xS$ solid solutions derived from their Zn atomic concentration.

1. Introduction

The conversion of solar energy into hydrogen via the water splitting process assisted by photo-semiconductor catalysts is one of the most interesting ways of achieving clean and renewable energy systems [1,2]. Among the available photo-semiconductors studied with the aim of storing solar energy as structured energy in H–H chemical bonds [3–7], CdS is an interesting photocatalyst material, since it has a narrow band gap (2.4 eV) and a suitable conduction band potential to effectively produce hydrogen from aqueous solutions. However, the photocatalytic properties of CdS are limited as a consequence of its photocorrosion under visible light irradiation. Nevertheless, there are strategies for reducing photocorrosion and increasing the photocatalyst efficiency of CdS. A common method consists in the use of suitable sacrificial reagents. A Na_2S/Na_2SO_3 mixture added to the water/semiconductor suspension is considered a very effective way of reducing the photocorrosion of CdS based catalysts [8–15]. Considerable efforts are still being made to improve the photocatalytic properties of CdS catalysts. Different strategies are reported in literature to modify the photoactivity properties of CdS: (i) control of particle size, (ii) addition of cocatalysts or, (iii) combination with different elements to form mixed photocatalysts. Among these, the combination of semiconductors of different band gap forming solid solutions is an interesting way for photoactivity control since the potentials of the conduction and valence bands of solid solutions shift successively with composition. The optoelectronic and structural properties of ZnS make this material interesting as semiconductor for combining with CdS. ZnS has a wide band gap of 3.2 eV that may improve the photoabsorption ability of CdS and ZnS may form a continuous series of solid solutions with CdS ($Cd_{1-x}Zn_xS$) where metal atoms are mutually substituted in the same crystal lattice [16–18]. Although much research has been done studying the structural and optical properties of $Cd_{1-x}Zn_xS$ solid solutions as colloidal nanocristals for optoelectronic applications [19–21] much less information is available in their application as photocatalyst for water splitting in microcrystalline form [11,22–24]. In these studies it has been shown that both optical properties and photocatalytic activity depend strongly on Zn composition in $Cd_{1-x}Zn_xS$ solid solutions. However in these studies the variation in Zn composition on CdS was too broad not allowing to establish a clear relationship among the solid solution structures and photocatalytic activities. For that reason, in this work we studied the structural and photo-optical changes associated with small changes in composition of $Cd_{1-x}Zn_xS$ solid solutions ($0.2 < x < 0.35$) and their influence in the photocatalytic properties for water splitting under visible light irradiation.

* Corresponding author. Fax: +34915854773.
E-mail address: r.navarro@icp.csic.es (R.M. Navarro).

0920-5861/$ – see front matter © 2008 Elsevier B.V. All rights reserved.
doi:10.1016/j.cattod.2008.09.024

2. Experimental

2.1. Catalyst preparation

$Cd_{1-x}Zn_xS$ solid solutions (x = 0.20, 0.25, 0.30 and 0.35) were prepared by coprecipitation of CdS and ZnS from aqueous solutions of Cd^{2+} ($Cd(CH_3COO)_2 \cdot 2H_2O$) and Zn^{2+} ($Zn(CH_3COO)_2 \cdot 2H_2O$) at 298 K using Na_2S as precipitating agent. The precipitates thus obtained were filtered and extensively washed with deionised water until the concentration of Na^+ ions in the filtrate solution was lower than 0.01 ppm, as determined by inductively coupled plasma emission spectroscopy. The precipitates were dried overnight at 383 K and subjected to thermal treatment under He flow at 973 K to improve crystallinity and to promote the formation of $Cd_{1-x}Zn_xS$ solid solution. According to nominal Zn concentration, samples were labelled as CZx (x = 20, 25, 30 and 35)

2.2. Catalyst characterization

The chemical composition of the catalysts was determined by inductively coupled plasma atomic emission spectroscopy (ICP-AES), using a PerkinElmer Optima 3300DV apparatus. The samples were first dissolved in acid solutions (a mixture of HF, HCl and HNO_3), microwaved for 15 min, and diluted to concentrations within the detection range of the instrument.

The specific surface areas of the catalysts were calculated by applying the BET method to the N_2 adsorption isotherms measured at liquid nitrogen temperature on a Micromeritics ASAP 2100 apparatus on samples previously degassed at 473 K for 24 h.

The morphology and size of the photocatalyst aggregates were observed by scanning electron micrographs taken using a JEOL-JSM-6700F field emission microscope.

X-ray diffraction patterns were recorded using a Seifert 3000P vertical diffractometer and nickel-filtered Cu Kα radiation (λ = 0.1538 nm) under constant instrument parameters. For each sample, Bragg angles between 5° and 80° were scanned. A rate of 5 s per step (step size: 0.04° 2θ) was used during a continuous scan in the abovementioned range. Volume-averaged crystallite sizes were determined by applying the Debye–Scherrer equation.

The UV–visible spectra of photocatalysts were measured on a Shimadzu UV2100 instrument equipped with a Labsphere diffuse reflectance accessory. Band gap size was obtained by plotting a tangent line over the slope of the UV–visible spectra and prolonging it to $f(R) = 0$. The wavelength value obtained was converted to [eV] given $E_{ph} = hc$, where h is the Plank constant and c the speed of light.

2.3. Catalytic activity measurements

The photocatalytic activity was determined in a pyrex cell connected to a gas-closed circulation system. The photocatalyst powder (0.1 g) was dispersed by magnetic stirring in an aqueous solution (150 mL) containing 0.05 M Na_2S/0.02 M Na_2SO_3 as sacrificial reagents. The photocatalyst was irradiated for 5 h with a Xe OF 300 W arc lamp (ILC technology; CERMAX LX-300) and optical filters for visible light irradiation. Samples of the evolved gases were extracted periodically and analyzed by GC with TCD (Ohkura 802, TCD) equipped with a 5 A molecular sieve using Ar as carrier gas.

3. Results

3.1. Chemical composition and textural properties

Table 1 displays the atomic Zn/Cd ratio obtained from ICP analyses of thermally treated CZx photocatalysts. As observed in Table 1, the chemical compositions measured for all samples were close to theoretical values indicating the efficiency of the precipitation method used in the preparation of the photocatalysts. Textural data in Table 1, indicate that the surface area of CZx samples varies with the Zn content in the formulation. All samples displayed low values of both surface area and pore volume with these findings supporting that photocatalysts do not develop a nanoporous structure. Furthermore, a decrease in surface area is observed with the increase in Zn concentration. This is indicative of structural changes and/or crystal growth induced by the presence of Zn in the formulation.

Table 1
Composition (atomic Zn/Cd ratio from ICP and EDX analyses) and textural data (from N_2 adsorption) of CZx photocatalysts.

	Zn/Cd (at/at)		BET (m^2/g)
	ICP	EDX	
CZ20	0.19	0.18	6.2
CZ25	0.25	0.29	4.6
CZ30	0.30	0.33	1.9
CZ35	0.36	0.34	2.5

3.2. Scanning electron microscopy

Fig. 1 reports SEM microphotograps of the CZx photocatalysts. As it is shown in SEM images, sheet-like aggregates of different sizes were formed depending on the Zn content in the solids, with the homogeneity and size of aggregates changing with the Zn content. One can notice that the sample with lowest Zn concentration (CZ20, Fig. 1a) forms aggregates with low homogeneity and particle sizes, in the range from 50 nm to 1 μm. Compared with this sample, the photocatalyst CZ30 (Fig. 1c) presents higher and more homogeneous aggregates while the samples CZ25 (Fig. 1b) and CZ35 (Fig. 1d) form well-shaped aggregates with sizes in the 0.3–1 μm range.

The chemical homogeneity of CZx samples was checked using EDX analyses on the aggregates. The numerical data of Zn/Cd ratio obtained from these analyses (Table 1) are close to that obtained from bulk ICP analyses indicating the homogeneous composition of the solid aggregates observed by SEM.

3.3. X-ray diffraction

The crystal structure of CZx photocatalysts was investigated by X-ray diffraction being the difractograms reported in Fig. 2. As it may be observed in Fig. 2, all samples exhibited reflections at 2θ angles of 24.8°, 26.5°, 28.2°, 36.6°, 43.7°, and 47.9° characteristic of hexagonal wurtzite CdS phase (JCPDS 77-2306) with lower lattice parameters (Table 2) than those observed for pure CdS hexagonal phase. The successive shift of the pattern (Fig. 2) indicates the formation of $Cd_{1-x}Zn_xS$ solid solutions by insertion of Zn ions into the CdS lattice [25–27]. The observed reduction of the lattice parameter with the increase in Zn concentration is the consequence of the improvement in the compact arrangement of atoms in the crystals. Since the lattice parameters of $Cd_{1-x}Zn_xS$ solid solutions follow Vergard's law [26,27], the successive decrease in lattice spacing (Fig. 3) is indicative of a change in the solid solution composition, with a higher degree of substitution of Zn in the CdS structure when the Zn concentration increases in the formulation. Solid solution compositions calculated by application of Vergard's law are reported in Table 2. From the calculated values of solid solution compositions (Table 2) it may be observed that, except for the sample with lower Zn concentration, the degree of introduction of Zn in the $Cd_{1-x}Zn_xS$ crystalline solid solution is almost complete for all samples. The variation of the size of $Cd_{1-x}Zn_xS$ particles

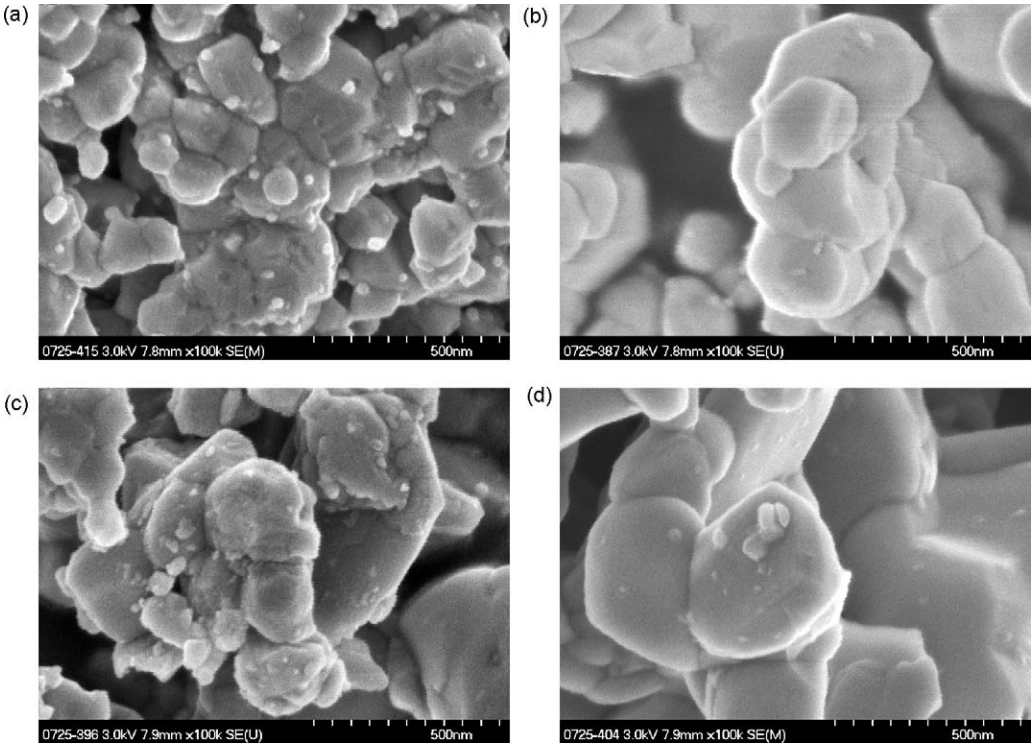

Fig. 1. SEM micrographs of CZ*x* photocatalysts: (a) CZ20, (b) CZ25, (c) CZ30 and (d) CZ35.

calculated from the Scherrer formula, applied to the (0 0 2) diffraction peak, was also calculated and the values are given in Table 2. As derived from this table, the crystalline size of solid solution particles increases gradually when the Zn concentration raises up to 0.3 decreasing subsequently when the Zn concentration becomes larger than 0.35. The observed variations in particle size were mainly associated to the presence of Zn in the crystals because the thermal treatment after solid precipitation to promote crystalline growth was identical for all samples.

Table 2
Lattice constants, particle size and composition of $Cd_{1-x}Zn_xS$ solid solution from XRD patterns of CZ*x* photocatalysts.

	Lattice parameters		*x*	dp (nm)
	a (Å)	*c* (Å)	$Cd_{1-x}Zn_xS$	$Cd_{1-x}Zn_xS$
CZ20	4.0988	6.6627	0.121	35
CZ25	4.0607	6.6064	0.241	45
CZ30	4.0423	6.5825	0.299	57
CZ35	4.0306	6.5630	0.336	52

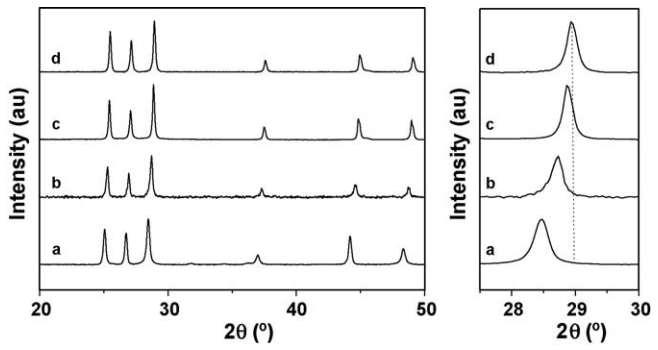

Fig. 2. XRD patterns of CZ*x* photocatalysts: (a) CZ20, (b) CZ25, (c) CZ30 and (d) CZ35.

3.4. UV–visible spectra

Fig. 4 shows the UV–visible absorption spectra of CZ*x* photocatalysts. The absorption edges of CZ*x* photocatalysts gradually shift from 510 nm to 485 nm as the Zn concentration increases. The band gap for each catalyst, calculated from the onsets of the absorption edges, is given in Table 3. One can notice that the band gap for all CZ*x* samples is higher than the value of 2.4 eV reported for pure crystalline CdS. The band gap size of CZ*x* photocatalysts displays a monotonous change in energy (from 2.49 eV to 2.68 eV) with this being a function of the Zn composition. The observed variation in the binding energy of CZ*x* photocatalysts may be caused, taking into account the factors that affect the band gap of semiconductors [28–30], by modifications in the solid solution composition and/or quantum effects due to variations in the size of the solid solution crystals.

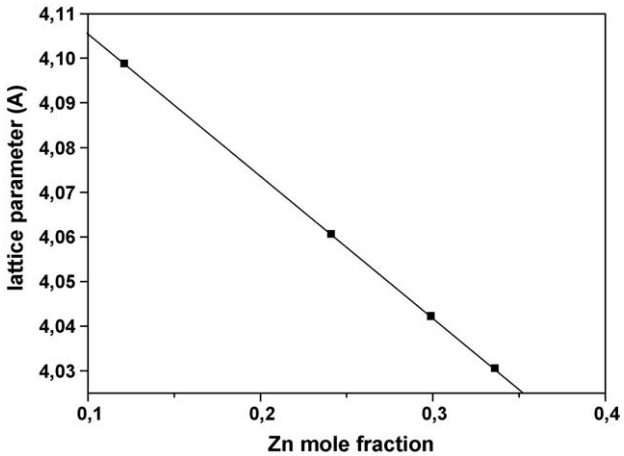

Fig. 3. Variation of lattice parameter of CZ*x* photocatalysts as function of Zn concentration (solid line: calculated data from Vegard's law).

Table 3
Band gap enery from UV–visible spectra of CZ*x* photocatalysts.

	Band gap (eV)
CZ20	2.49
CZ25	2.58
CZ30	2.64
CZ35	2.68

3.5. Photocatalytic activity

Fig. 5 reports the hydrogen evolution rate under visible light irradiation over CZ*x* photocatalysts. All CZ*x* samples showed relatively high activities for hydrogen evolution with hydrogen formation rates much higher than those obtained with the CdS reference sample prepared using the same procedure than for the CZ*x* counterparts. One should also notice that among the CZ*x* photocatalysts, significant differences in activity were observed, with this being a function of the Zn concentration in the samples. As Fig. 4 shows, hydrogen production rates were found to increase gradually when the Zn concentration on photocatalysts increases from 0.2 to 0.3. Subsequent increases in the Zn concentration up to 0.35 lead to lower hydrogen production. The observed changes in the photocatalytic activity are hypothesized to be a consequence of the changes on semiconductor structure, conduction band level, absorption of photons, mobility of the photogenerated carriers, etc. associated with the variation in Zn concentration in photocatalysts that will be discussed in the next section.

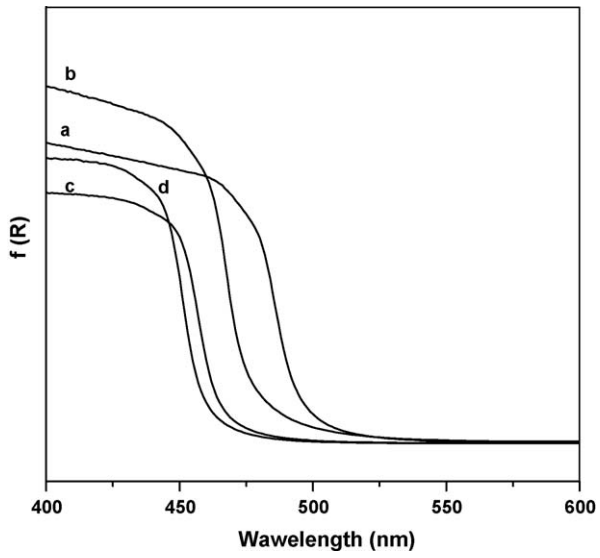

Fig. 4. UV–vis spectra of CZ*x* photocatalysts: (a) CZ20, (b) CZ25, (c) CZ30 and (d) CZ35.

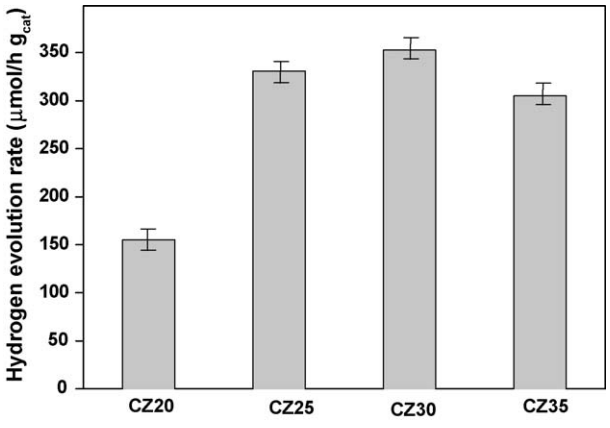

Fig. 5. Hydrogen evolution rate from aqueous solution containing $Na_2S + Na_2SO_3$ under visible light irradiation over CZ*x* photocatalysts.

4. Discussion

The specific structure and energy bands of visible-light-driven photocatalyst affect the generation and effective utilization of electron and holes involved in hydrogen photo production. In this respect, the development of CdS solid solutions with Zn inclusion is the strategy adopted in this study to control the energy structure of CdS.

The physicochemical characterization of CZ*x* photocatalysts prepared in this study shows that the variation in Zn concentration induces significant structural and photo-optical changes on the samples. As it can be observed in Fig. 2, the CZ*x* photocatalysts display well crystallized $Cd_{1-x}Zn_xS$ solid solution with hexagonal wurtzite structure. The composition of crystalline $Cd_{1-x}Zn_xS$ solid solutions derived from Vergard's law (Table 2) was close to the chemical bulk composition (Table 1), except for the sample with the lowest Zn concentration. This shows the effectiveness of the coprecipitation procedure, used in this study, to form $Cd_{1-x}Zn_xS$ solid solutions with a relatively high crystallinity. In spite that all samples were annealed at the same temperature, differences in the size of $Cd_{1-x}Zn_xS$ crystallites were observed. Crystalline size of solid solution particles increases gradually with Zn up to 0.3, decreasing subsequently when the Zn concentration exceeds 0.35 (Table 2).

Although the mechanism of precipitation and thermal formation of $Cd_{1-x}Zn_xS$ solid solutions are quite poorly understood, the observed changes in crystallite size of solid solutions with Zn loading may be associated to the reduction of Cd^{2+} ion concentration in the precipitate solution which is expected to affect the rate of precipitation of the host CdS leading to precipitates of different size [31,32]. The variation in size of $Cd_{1-x}Zn_xS$ crystals is consistent with the observed surface area of the photocatalysts (Table 1). This indicates that the photocatalyst exposed surface area is mainly the result of the geometric areas of the $Cd_{1-x}Zn_xS$ solid solution crystals.

The changes in Zn composition of photocatalysts have effect on their photophysical properties with a monotonous variation in band gap size with the increase in the Zn atomic fraction (Table 3). Literature references [28–30] have stated that the variation in the band gap of a semiconductor is determined by the following factors: (i) inherent band gap of the material and (ii) quantum size effects (by decreasing the particle size, the fundamental band edges shift towards the blue). The quantum confinement effect appears when the crystallite size of semiconductors is smaller than the Bohr radii of the excitons. Changes in band gap associated to quantum confinement effect can be excluded in the CZ*x* samples because the size of $Cd_{1-x}Zn_xS$ crystals in photocatalysts is larger than the corresponding Bohr exciton radius for CdS (3.0 nm [33]). Therefore, the significant band gap energy increase observed for CZ*x* photocatalysts mainly arises from the compositional variation of $Cd_{1-x}Zn_xS$ crystalline solid solution instead of a size effect. To corroborate that, the bulk band gap energy for $Cd_{1-x}Zn_xS$ solid solution may be theoretically calculated by the equation $E_g(x) = 2.5 + 0.59x + 0.61x^2$ (eV), where x is the atomic fraction of Zn [34,35]. From this equation, the theoretical values of band gap as a function of the Zn content for the $Cd_{1-x}Zn_xS$ crystals are depicted in Fig. 6. As it is observed in this figure, the experimental variation of binding energy for CZ*x* phototocatalysts fits very well

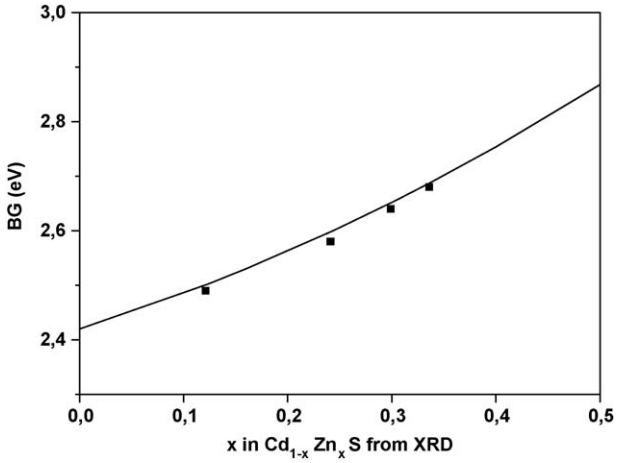

Fig. 6. Band gap energy as a function of the Zn composition (x) in the $Cd_{1-x}Zn_xS$ solid solutions (square points: experimental data, solid line: empirical relationship).

with the empirical relationship for bulk $Cd_{1-x}Zn_xS$ calculated for the Zn concentration values derived from XRD analyses. The continuous shift in band gap energy with Zn content agrees well with the trend expected for similar sulfide solid solutions [36] in which the change in band gap energy is associated to an increase in the position of the conduction band by the hybridization of Cd 5s5p level with the more negative Zn 4s4p level.

As previously indicated, the photophysical properties and the effective utilization of photogenerated carriers are crucial factors influencing the activity of photocatalysts. The photophysical properties, as light absorption and position of conduction and valence bands, are associated to photocatalyst composition while the effective utilization of carriers is mainly governed by the crystallinity and surface morphology of photocatalysts. High photocatalytic activities are associated to: (i) high visible light absorption with a conduction band level higher than reduction H^+/H_2 potential and, (ii) a low electron/hole recombination. Wider band gap decreases the light absorption of photocatalysts but can also elevate the conduction band gap position of the resulting solid solution. Therefore, there is a delicate balance between light absorption and the reduction power of conduction band that is necessary to be kept in the phtotocatalysts. Concerning the control of electron/hole recombination, it is necessary to achieve phtotocatalyst phases with good crystallinity and few crystal defects.

According to the above described factors, the variation in photoactivity observed for the samples (Fig. 5) may be the consequence of the modification of the particle size and photo-absorption properties of CZ*x* samples. The physicochemical characterization of the photocatalysts of this study shows that the prepared samples were mainly composed of $Cd_{1-x}Zn_xS$ solid solutions with different composition and crystalline size. The increase of the energy level of the conduction band, formed by hybridized Zn 4s4p and Cd 5s5p levels, together with the increase in particle size when Zn concentration in photocatalysts is raised from 0.2 to 0.25 may explain the sharp augmentation in photoactivity observed in the CZ25 sample (Fig. 5). The increase in photoactivity when the Zn fraction is raised up to 0.3 was moderate and this in spite of the increase in particle size and energy level of the conduction band achieved in this sample (Tables 2 and 3). The explanation for this moderate increase in activity may be related with the counteracting effect of the decrease of available photons associated to the increase in the band gap of the photocatalyst [37]. In line with this appears the photoactivity reduction observed for the sample with Zn fraction of 0.35 (CZ35, Fig. 5). Accordingly, the lower activity observed for CZ35 sample is considered to be primarily due to the decrease of available photons, a result of the high band gap of this photocatalyst. Additionally, the decrease in particle size of the Cd–Zn solid solution also contributes to the lower activity observed in this sample. Therefore, the crystallinity degree and a balance between the level of conduction band and the light absorption ability of Cd–Zn solid solutions govern their photactivity for H_2 production under visible light. It is hypothesized that the balance between these properties that lead to higher photoactivity was achieved for the $Cd_{0.7}Zn_{0.3}S$ solid solution composition.

5. Conclusions

The control of the energy structure of CdS by making solid solutions with Zn ($Cd_{1-x}Zn_xS$ $0.2 < x < 0.35$) was investigated for its application in hydrogen production involving aqueous solutions containing SO_3^{2-}/S^{2-} as sacrificial reagents under visible light. The variation of composition of $Cd_{1-x}Zn_xS$ solid solutions leads to changes in their: (i) crystallinity degree, (ii) level of conduction band and, (iii) light absorption ability associated to changes in band gap. It is shown that changes in optical and structural characteristics of $Cd_{1-x}Zn_xS$ solid solutions influence photocatalytic activity. The photocatalytic activity of $Cd_{1-x}Zn_xS$ solid solutions increases gradually when the Zn concentration in photocatalyst grows to 0.3 and decreases subsequently when the Zn concentration rises up to 0.35. The enhancement of activity with the increase of Zn concentration up to 0.3 is explained in terms of the higher particle size and higher energy level of the conduction band of solid solution formed, while the decrease in activity for the sample with Zn concentration of 0.35 is attributed to a decrease in the number of available photons with widening of the band gap and increase in solid solution crystallite sizes.

Acknowledgements

We are grateful to our research sponsors CICyT and CAM (Spain) under grants ENE2007-67533-C02-01 and S-0505/EN/0404, respectively. FV would like to acknowledge CONACYT (Mexico) for the research grant, MCSS and JAVM acknowledge the Comunidad de Madrid for their research grant.

References

[1] F.E. Osterloh, Chem. Mater. 20 (2008) 35.
[2] K. Rajeshwar, J. Appl. Electrochem. 37 (2007) 765.
[3] R. Konta, T. Ishi, H. Kato, A. Kudo, J. Phys. Chem. B 108 (2004) 8992.
[4] H. Kato, K. Asakura, A. Kudo, J. Am. Chem. Soc. 15 (2003) 3082.
[5] A. Kudo, K. Omorin, H. Kato, J. Am. Chem. Soc. 121 (1999) 11459.
[6] G. Hitoki, T. Tataka, J.N. Kondo, M. Hara, K. Kobayashi, K. Domen, J. Phys. Chem. A 106 (2002) 6750.
[7] K. Maeda, T. Takata, M. Hara, N. Saito, Y. Inoue, H. Kobayashi, K. Domen, J. Am. Chem. Soc. 127 (3) (2005) 8286.
[8] J.R. Darwent, G. Porter, J. Chem. Soc. Chem. Commun. 4 (1981) 145.
[9] M. Matsumura, Y. Sato, H. Tsubomura, J. Phys. Chem. 87 (1983) 3807.
[10] L. Borrell, S. Cervera-March, J. Gimenez, R.A. Simarro, Sol. Energy Mater. Sol. Cells 25 (1992) 25.
[11] J.F. Rebel, K. Meier, J. Phys. Chem. 90 (1986) 824.
[12] A.S.K. Sinha, S. Namita, M.K. Arora, S.N. Upadhayay, Catal. Today 69 (2001) 297.
[13] M.R. Hoffmann, S.T. Martin, W. Choi, D.W. Bahnemann, Chem. Rev. 95 (1995) 69.
[14] M. Sathish, B. Viswanathan, R.P. Viwanath, Int. J. Hydrogen Energy 31 (2006) 891.
[15] T. Inue, T. Watanabe, A. Fujishima, K. Honda, K. Kohayakawa, J. Electrochem. Soc. 124 (1977) 719.
[16] V.A. Fedorov, V.A. Ganshing, Y.U.N. Norkeshko, Mater. Res. Bull. 28 (1993) 50.
[17] T.L. Chu, S.S. Chu, J. Britt, C. Ferekides, C.Q. Wu, J. Appl. Phys. 70 (1991) 2688.
[18] A. Nayeem, K. Yadaiah, G. Vajralingam, P. Mahesh, M. Nagabhooshanam, Int. J. Mod. Phys. B 15 (7) (2001) 2387.
[19] X. Zhong, Y. Feng, W. Knoll, M. Hang, J. Am. Chem. Soc. 125 (2003) 13559.
[20] Y.J. Hsu, S.Y. Lu, Y.F. Lin, Adv. Funct. Mater. 15 (2005) 1350.

[21] Y. Li, M. Ye, C. Yang, X. Li, Y. Li, Adv. Funct. Mater. 15 (2005) 433.
[22] N. Kakuta, K.H. Park, M.F. Finlayson, A. Ueno, A.J. Bard, A. Campion, M.A. Fox, S.E. Webber, J.M. White, J. Phys. Chem. 89 (1985) 732.
[23] C. Xing, Y. Zhang, W. Yan, L. Guo, Int. J. Hydrogen Energy 31 (2006 2018).
[24] K. Zang, D. Jing, C. Xing, L. Guo, Int. J. Hydrogen Energy 32 (2007) 4685.
[25] M.T. Sebastian, P. Krishna, Solid State Commun. 48 (1983) 879.
[26] A. Nayeem, K. Yadaiah, G. Vajralingam, P. Mahesh, M. Nagabhooshanam, Int. J. Mod. Phys. B 16 (3) (2002 481).
[27] P. Cherin, E.L. Lind, E.A. Davis, J. Electrochem. Soc. 117 (2) (1970) 233.
[28] R. Rossetti, R. Hull, J.M. Gibson, L.E. Brus, J. Chem. Phys. 80 (1984) 4464.
[29] M. Ichimura, F. Goto, E. Arai, J. Appl. Phys. 58 (10) (1999) 7411.
[30] O. Zelaya-Angel, A.E. Esparza-García, C. Falcony, R. Lozada-Morales, Solid State Commun. 94 (1) (1995) 81.
[31] H. Weller, Angew. Chem. Int. Ed. Engl. 32 (1993) 41.
[32] C. Numako, I. Nakai, Spectrochim. Acta Part B 54 (1999) 133.
[33] X.H. Zhong, Y.Y. Feng, W. Knoll, M.Y. Han, J. Am. Chem. Soc. 125 (2003) 13559.
[34] J. Cizeron, M.P. Pileni, J. Phys. Chem. 99 (1995) 17410.
[35] D.V. Petrov, B.S. Santos, G.A.L. Pereira, C.M. Donegaa, J. Phys. Chem. B 106 (2002) 5325.
[36] I. Tsuji, H. Kato, H. Kobayashi, A. Kudo, J. Am. Chem. Soc. 126 (2004) 13406.
[37] T. Bak, J. Nowotny, M. Rekas, C.C. Sorrell, Int. J. Hydrogen Energy 27 (2002) 991.